Desalination and Water Treatment
www.deswater.com

doi: 10.5004/dwt.2017.20845

81 (2017) 26–32
June

Dimensional analysis and numerical simulation methods for the influence of impellers on the average velocity of flows in an oxidation ditch

Yuling Liu, D. Li, W. Wei*, B. Lv, J. Wei

State Key Laboratory base of Eco-Hydraulic Engineering in Arid Area (SKLEHE), Xi'an University of Technology, Xi'an 710048, Shaanxi, China, Tel. +86 15596886263; email: wwl_p@126.com (W. Wei), Tel. +86 18591999882; email: 29992359@qq.com (Y. Liu), Tel. +86 18792767628; email: 734602890@qq.com (D. Li), Tel. +86 15191913820; email: binlv @126.com (B. Lv), Tel. +86 18629352022; email: jwei1995@126.com (J. Wei)

Received 7 September 2016; Accepted 20 April 2017

ABSTRACT

Running impellers have a great influence on the velocity distribution and the flow structure in an oxidation ditch (OD). In this paper, the dimensional analysis and computational fluid dynamics methods were used to study the influence of rotational speed of impellers on the average velocity of the flow in an OD. The time-averaged Navier–Stokes (N–S) equations with a three-dimensional (3D) renormalized group (RNG) k–ε turbulence model were solved by FLUENT6.3.26 for the velocity and pressure fields. By the dimensional analysis and simulation results, the relation between the rotational speed of impellers and the average velocity of the flow was obtained, which can provide a reference in the designing of ODs.

Keywords: Oxidation ditch; Rotational speed of impellers; Dimensional analysis; CFD; Average velocity of the flow

1. Introduction

Oxidation ditch (OD) is one of the widely used wastewater treatment reactors. There are several different kinds of ODs, such as integrative OD, Orbal OD and Carrousel OD. The flow hydrodynamic characteristics playing a significant role in the design and operation of ODs have much been studied by numerical simulations. Wang et al. [1] used Fluent to simulate the velocity distribution of flows in bend channels of an OD to investigate the type of guide walls for reducing sludge deposition. Chen and Yang [2] proposed a novel corrugated plate as a guide wall for an OD, and simulated the flow patterns and flow velocity distribution in the OD by the numerical solution of the Reynolds time-averaged equations and a turbulent model, which shows that the corrugated-plate guide wall can reduce the lower speed region and prevent sludge deposition. Li et al. [3] simulated the flow fields in a deep OD with a guide plate downstream of a disk aerator by computational fluid dynamics (CFD) to study the influence of the guide plate on flow patterns, and proposed reasonable parameters for the designing and installation of the guide plate. Fan et al. [4] focused on the hydrodynamics of ODs by experiments and simulations. The 3D two-phase liquid–solid flow fields in an OD aerated with surface aerators like an inverse umbrella were simulated with CFD, and the simulated results are in good agreement with experiments. The liquid and solid phases have a similar flow velocity, while the vertical velocity of the solid phase is slightly lower than that of liquid. With the increase of aerator speed, the flow velocity increases and the solid phase disperses more evenly. Li and Ni [5] developed a 3D three-phase fluid model to simulate the hydrodynamics, oxygen mass transfer, carbon oxidation, nitrification and denitrification processes in an OD. The model provided the detailed phase information on the liquid flow field, gas hold-up distribution and sludge sedimentation. The three-phase model can describe water–gas, water–sludge and gas–sludge interactions. Yang et al. [6] proposed an experimentally validated numerical tool, based on CFD model, to optimize the operating condition by

* Corresponding author.

considering two important factors: flow field and dissolved oxygen concentration profiles. The model is capable of predicting flow patterns and oxygen mass transfer characteristics in ODs equipped with surface aerators and submerged impellers. Liu et al. [7] proposed a new control model feasible online implemented by programmable logic controller to enhance nitrogen removal against the fluctuation of influent in Carrousel ODs. The discrete-time control model was established by confirmation model of operational conditions based on an expert access, which was obtained by a simulation using CFD, Activated Sludge Model 2D and discrete-time control model to switch between different operational stages. Tang et al. [8] proposed a new 3D submerged propeller model along with the RNG *k*–ε turbulence model and a multiple reference frame (MRF) model for simulating the flow fields in an OD, by which the velocity distribution and flow patterns in an OD were successfully and effectively simulated. Yang et al. [9] used a CFD technique along with a Fluent code to perform a two-dimensional (2D) simulation of the single-phase flow in an integrated OD with a vertical circle, by which the effect of the guide-plate structure on the velocity distribution in the bend channel was explored. The simulation results indicate that the flow pattern varies substantially with the different guide-plate structures under the same boundary conditions. Luo et al. [10] used a 3D *k*–ε turbulence model to simulate the flow fields in a small-scale operational ditch, and the simulated results are in agreement with the measured data. Xie et al. [11] developed a two-phase (liquid–solid) CFD model for simulating the flow fields and sludge settling in a full-scale Carrousel OD. Based on the simulation results of the flow fields and sludge settling, an optimized operation scheme of the OD was proposed.

The references [1–11] mainly study the physical properties of a single-phase or two-phase flow in an OD, but do not deal with the influence of impellers on the average velocity of the flows. Impellers have an important influence on the flow velocity distribution and flow structure in an OD. When the radius of impellers is fixed at a constant, the larger the rotational speed of impellers is, the greater is the average velocity over a cross-section. Thus, a proper rotational speed of impellers should be proposed for an OD to obtain the ideal flow so that the efficiency of water treatment will be increased. Therefore, the objective of this work is to find the variation of average velocity over a cross-section with the rotational speed of impellers by the dimensional analysis method and the solution of time-averaged N–S equations along with a 3D RNG *k*–ε turbulence model, which can provide a reference in the designing of ODs.

2. Dimensional analysis of the variation of average velocity of the flow with the rotational speed of impellers

After analysis, it is known that the average velocity over a cross-section (V) in an OD is related to the following physical parameters: the rotational speed of impellers (ω), the density of water (ρ), the gravity acceleration (g), the viscosity of water (ν), the width of the straight channel (B), the water depth (H), the radius of impellers (r) and the radius of small bends (R_1). Therefore, the formula for the average velocity (V) can be written as:

$$V = f(\omega,\rho,g,\nu,B,H,r,R_1) \tag{1}$$

in which there are nine variables, including one dependent variable V and eight independent variables ω, ρ, g, ν, B, H, r and R_1. The three physical quantities, ω, ρ and g, are selected as the repeating variables, so the formula for the relationship between nine dimensionless numbers (π) can be expressed as [12]:

$$\pi = f(\pi_1,\pi_2,\pi_3,\pi_4,\pi_5,\pi_6,\pi_7,\pi_8) \tag{2}$$

where the nine dimensionless numbers (π) are:

$$\begin{aligned}
&\pi = \frac{V}{\omega^{x_0}\rho^{y_0}g^{z_0}},\ \pi_1=\pi_2=\pi_3=1,\\
&\pi_4 = \frac{\nu}{\omega^{x_4}\rho^{y_4}g^{z_4}},\ \pi_5 = \frac{B}{\omega^{x_5}\rho^{y_5}g^{z_5}},\\
&\pi_6 = \frac{H}{\omega^{x_6}\rho^{y_6}g^{z_6}},\ \pi_7 = \frac{r}{\omega^{x_7}\rho^{y_7}g^{z_7}},\\
&\pi_8 = \frac{B_1}{\omega^{x_8}\rho^{y_8}g^{z_8}}.
\end{aligned} \tag{3}$$

Because π is a dimensionless number, the dimensions of the physical quantities are written in the dimensions of length L, time T and mass M as:

$$\left.\begin{aligned}
&\dim V = \dim \omega^{x_0}\rho^{y_0}g^{z_0}\\
&\dim \nu = \dim \omega^{x_4}\rho^{y_4}g^{z_4}\\
&\dim B = \dim \omega^{x_5}\rho^{y_5}g^{z_5}\\
&\dim H = \dim \omega^{x_6}\rho^{y_6}g^{z_6}\\
&\dim r = \dim \omega^{x_7}\rho^{y_7}g^{z_7}\\
&\dim R_1 = \dim \omega^{x_8}\rho^{y_8}g^{z_8}
\end{aligned}\right\} \Rightarrow \left\{\begin{aligned}
&LT^{-1}=L^{-3y_0+z_0}M^{y_0}T^{-x_0-2z_0}\\
&L^2T^{-1}=L^{-3y_4+z_4}M^{y_4}T^{-x_4-2z_4}\\
&L=L^{-3y_5+z_5}M^{y_5}T^{-x_5-2z_5}\\
&L=L^{-3y_6+z_6}M^{y_6}T^{-x_6-2z_6}\\
&L=L^{-3y_7+z_7}M^{y_7}T^{-x_7-2z_7}\\
&L=L^{-3y_8+z_8}M^{y_8}T^{-x_8-2z_8}
\end{aligned}\right\} \tag{4}$$

The exponents of each dimension must be the same on both sides of the equations, so the following equations can be obtained:

$$\begin{aligned}
&\begin{cases}1=-3y_0+z_0\\0=y_0\\-1=-x_0-2z_0\end{cases} \Rightarrow \begin{cases}x_0=1\\y_0=0\\z_0=1\end{cases} \Rightarrow \pi = \frac{V}{\omega^{x_0}\rho^{y_0}g^{z_0}} = \frac{V}{\omega^{-1}g}\\
&\begin{cases}2=-3y_4+z_4\\0=y_4\\-1=-x_4-2z_4\end{cases} \Rightarrow \begin{cases}x_4=-3\\y_4=0\\z_4=2\end{cases} \Rightarrow \pi_4 = \frac{\nu}{\omega^{x_4}\rho^{y_4}g^{z_4}} = \frac{\nu}{\omega^{-3}g^2}\\
&\begin{cases}1=-3y_5+z_5\\0=y_5\\0=-x_5-2z_5\end{cases} \Rightarrow \begin{cases}x_5=-2\\y_5=0\\z_5=1\end{cases} \Rightarrow \pi_5 = \frac{B}{\omega^{x_5}\rho^{y_5}g^{z_5}} = \frac{B}{\omega^{-2}g}\\
&\begin{cases}1=-3y_6+z_6\\0=y_6\\0=-x_6-2z_6\end{cases} \Rightarrow \begin{cases}x_4=-2\\y_4=0\\z_4=1\end{cases} \Rightarrow \pi_6 = \frac{H}{\omega^{x_6}\rho^{y_6}g^{z_6}} = \frac{H}{\omega^{-2}g}\\
&\begin{cases}1=-3y_7+z_7\\0=y_7\\0=-x_7-2z_7\end{cases} \Rightarrow \begin{cases}x_7=-2\\y_7=0\\z_7=1\end{cases} \Rightarrow \pi_7 = \frac{r}{\omega^{x_7}\rho^{y_7}g^{z_7}} = \frac{r}{\omega^{-2}g}\\
&\begin{cases}1=-3y_8+z_8\\0=y_8\\0=-x_8-2z_8\end{cases} \Rightarrow \begin{cases}x_8=-2\\y_8=0\\z_8=1\end{cases} \Rightarrow \pi_8 = \frac{R_1}{\omega^{x_8}\rho^{y_8}g^{z_8}} = \frac{R_1}{\omega^{-2}g}
\end{aligned} \tag{5}$$

Substituting the above π dimensionless numbers into the dimensionless governing Eq. (2) yields:

$$\frac{V}{\omega^{-1}g} = f\left(1,1,1,\frac{\nu}{\omega^{-3}g^{2}},\frac{B}{\omega^{-2}g},\frac{H}{\omega^{-2}g},\frac{r}{\omega^{-2}g},\frac{R_1}{\omega^{-2}g}\right) \tag{6}$$

Therefore,

$$V = \varphi\frac{g}{\omega} \tag{7}$$

where ϕ is dimensionless number, and $\varphi = f(1,1,1,\frac{\nu}{\omega^{-3}g^{2}},\frac{B}{\omega^{-2}g},\frac{H}{\omega^{-2}g},\frac{r}{\omega^{-2}g},\frac{R_1}{\omega^{-2}g})$. Eq. (7) is the relationship between the variation of average velocity over a cross-section (V) with the rotational speed of impellers (ω).

3. Simulation and analysis of the variation of average velocity with the rotational speed of impellers

3.1. Governing equations

In most engineering practice, the time-averaged properties of flows are enough to provide the required information, which are obtained by solving the time-averaged equations for the flows in a whole range of turbulent scales to be modeled [13]. Thus, this modeling approach can greatly reduce required computational efforts and resources, and is widely adopted for practical engineering applications [14,15].

The unsteady incompressible flow is described by the time-averaged mass and momentum conservation equations, and can respectively be written as [13]:

$$\frac{\partial\rho}{\partial t} + \frac{\partial(\rho u_i)}{\partial x_i} = 0 \tag{8}$$

and

$$\frac{\partial(\rho u_i)}{\partial t} + \frac{\partial(\rho u_i u_j)}{\partial x_j} = -\frac{\partial p}{\partial x_i} + \frac{\partial}{\partial x_j}\left[\mu\left(\frac{\partial u_i}{\partial x_j} + \frac{\partial u_j}{\partial x_i}\right)\right] - \frac{\partial}{\partial x_j}\left(\rho\overline{u_i' u_j'}\right) + \rho g_i \tag{9}$$

where ρ is density; t is time; x_i is the space coordinate in i-th direction; p is pressure; μ is molecular kinematic viscosity; μ_t is kinematic viscosity; g_i is the gravitational acceleration in i-th direction; u_i and U_i' are the time-averaged and fluctuating velocity components in i-th direction, respectively; and the subscripts i, j = 1, 2, 3.

The Reynolds-averaged N–S equations are always closed by the principal turbulence models, such as the standard k–ε model, and the relatively improved models named by the RNG and the realizable k–ε models in popular CFD [16–18].

The term, $-\rho\overline{u_i' u_j'}$, in Eq. (9) is defined as Reynolds stress, and must be modeled. In all the two-equation turbulence models, the modeling approach of Reynolds stress always assumes a locally isotropic turbulence, and employs the Boussinesq hypothesis relating these stresses to the mean deformation rates and mean velocity gradients [19]:

$$-\rho\overline{u_i' u_j'} = \mu_t\left(\frac{\partial u_i}{\partial x_j} + \frac{\partial u_j}{\partial x_i}\right) - \frac{2}{3}\left(\rho k + \mu_t\frac{\partial u_i}{\partial x_i}\right)\delta_{ij} \tag{10}$$

where μ_t is the turbulent viscosity, and computed as a function of turbulent kinetic energy k and kinetic energy dissipation rate ε [19]:

$$\mu_t = \rho C_\mu\frac{k^2}{\varepsilon} \tag{11}$$

where C_μ is a model constant with a value of 0.085.

In the RNG k–ε turbulence model, the transport equations for k and ε are given as [13,16–18]:

$$\frac{\partial(\rho k)}{\partial t} + \frac{\partial(\rho k u_i)}{\partial x_i} = \frac{\partial}{\partial x_j}\left[\left(\mu + \frac{\mu_t}{\sigma_k}\right)\frac{\partial k}{\partial x_j}\right] + G_k - \rho\varepsilon \tag{12}$$

and

$$\frac{\partial(\rho\varepsilon)}{\partial t} + \frac{\partial(\rho\varepsilon u_i)}{\partial x_i} = \frac{\partial}{\partial x_j}\left[\left(\mu + \frac{\mu_t}{\sigma_\varepsilon}\right)\frac{\partial\varepsilon}{\partial x_j}\right] + C_1\frac{\varepsilon}{k}G_k - \rho C_2\frac{\varepsilon^2}{k} \tag{13}$$

where σ_k, C_2 and σ_ε are empirical constants and have the values of 0.7179, 1.68 and 0.7179, respectively; and other parameters are: $C_{1\varepsilon}^{*} = C_{1\varepsilon} - \eta(1-\eta/\eta_0)/(1+\beta\eta^3)$, $\tilde{\eta} = Sk/\varepsilon, S = (2S_{i,j}S_{i,j})^{\frac{1}{2}}, \tilde{\eta}_0 = 4.38, \beta = 0.015,$ and $S_{i,j} = (\partial u_i/\partial x_j + \partial u_j/\partial x_i)/2$.

3.2. Calculated model and grid generation

The side wall of the Carrousel OD has a height of 5 m. The water depth is 4.5 m. The OD consists of four channels and four bends. The radius of the three small bends is 8.5 m, and of the big bend is 17 m. The four channels are, respectively, named A, B, C and D, each of which has a width of 8.5 m. The simulated domain has a length of 109 m, a width of 34.6 m and a height of 6 m. The thickness of the walls is 0.2 m. The capacity of the wastewater treatment is 25,000 m^3/d. There are three impellers installed at both ends of the OD. In the numerical calculation, the details of the calculation region are shown in Fig. 1.

Figs. 2(a) and (b) show the 3D grid and the 2D horizontal plan grid of the computational domain, which were generated by the GAMBIT procedure. The control Eqs. (8), (9), (12) and (13) were discretized by the finite volume method, and solved by the pressure-implicit with splitting of operators algorithm for the velocity and pressure fields.

3.3. Initial and boundary conditions

It was found that the flow inlet and outlet conditions for an OD have little influence on the flow field, so they were ignored in the numerical calculation [20]. Water flow in an OD has a free water surface, and the water surface is nearly taken as a plane above which there is air. Thus, the water

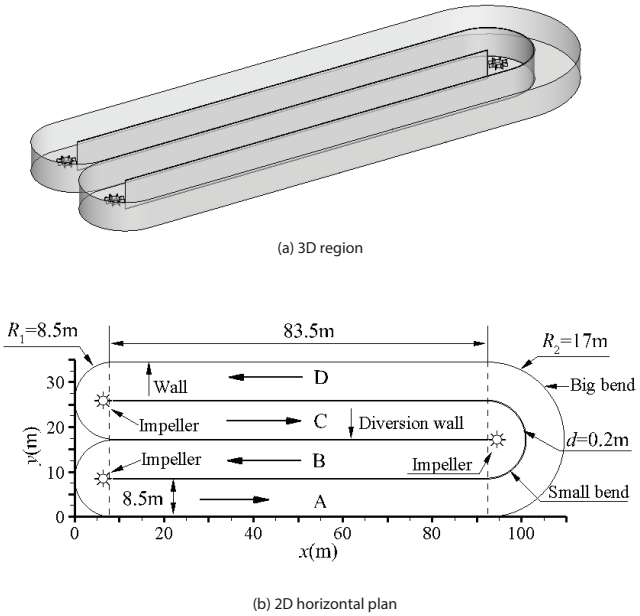

Fig. 1. Computational domain (a) 3D region and (b) 2D horizontal plan.

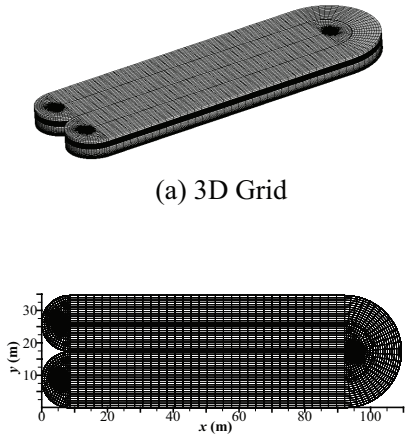

Fig. 2. Grids of the computational domain (a) 3D grid and (b) 2D horizontal plan grid.

surface is assumed to be flat so that the boundary condition for it could be given by a "rigid-lid" method. The boundary condition of the side walls and bottom is given by the wall-function. The initial condition is given as a stationary water depth. The rotational speed of submerged impellers is specified at 3.14, 4.19, 5.24, 6.28 and 7.33 rad/s, respectively.

The motion of the submerged impellers relative to an OD is described by a MRF model. In the computation with MRF, the computational domain is divided into two parts, (a) and (b), as shown in Fig. 3. Part (a) contains a moving blade and part (b) is the total computational region except part (a).

The two regions, (a) and (b), are calculated using two different reference coordinate systems, respectively. The region (a) with blades uses the reference system with the rotational speed of the blades; and part (b) uses the static reference frame. The velocity matching of the two different reference frames is done by the conversion of their interface. The equation of the velocity conversion is:

$$W = W_r + \omega \times r \tag{14}$$

$$\nabla W = \nabla W_r + \nabla(\omega \times r) \tag{15}$$

where W is the velocity of the stationary reference frame, W_r is the velocity of the rotating reference frame and ω is the rotation angular velocity.

3.4. Analysis of the simulated results

OD is a structure composed of bend and straight channels (Fig. 1). The smaller average velocity of the flow may cause sludge-phase retention in an OD, which is adverse to its operation. The rotational speed of impellers has a great influence on the average velocity. Here, the average velocity under different rotational speeds, 3.14, 4.19, 5.24, 6.28 and 7.33 rad/s, of impellers was simulated. The simulated velocity fields on the horizontal plane with submerged depth to the total water depth of 0.45 are shown in Fig. 4.

Fig. 4 shows that the recirculation zones near the end of straight walls are small with a smaller rotational speed of impellers, and continuously increase with an increasing in the rotational speed, which is mainly because the velocity at a point on the impeller blade increases with an increase in the rotational speed of impellers. This results in a very uneven velocity distribution at the bend outlets. The velocity is small near the straight wall and is great away from the straight wall, and at the bend outlet the effect of inertia force also causes an uneven velocity distribution. Therefore, the two aspects lead to a recirculation zone, and its length is much affected by the uneven velocity distribution at the bend outlets. The greater the rotational speed of impellers is, the more uneven is the velocity distribution, and the longer is the recirculation zone. At the same time, with an increase in rotational speed of impellers, the entrainment effect of the surrounding water will be enhanced, which has a great influence on the flow structure of the OD. Therefore, it is known that a larger rotational speed of impellers can generate a larger velocity distribution and a larger recirculation zone. For this OD, the simulated average velocities of the flows with different rotational speeds of impellers are shown in Table 1.

In Table 1, according to the simulated average velocities of the flows with different rotational speeds of impellers, the fitting line is obtained as shown in Fig. 5 and the relationship for the variation of V with g/ω is written as:

$$v = -0.485\frac{g}{\omega} + 1.956 \tag{16}$$

with g/ω in the reference range of $1.34 < g/\omega < 3.0$, which shows that the variation of average velocities of the flows with different rotational speeds of impellers is nearly in a linear relationship.

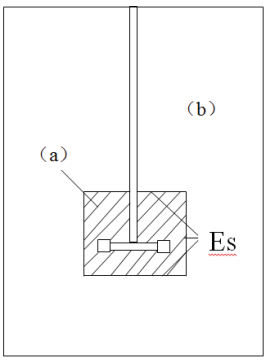

Fig. 3. Sketch of MRF(a) the internal region (using a rotating coordinate system); (b) the external region (using a stationary coordinate system); Es, the interface of the two part.

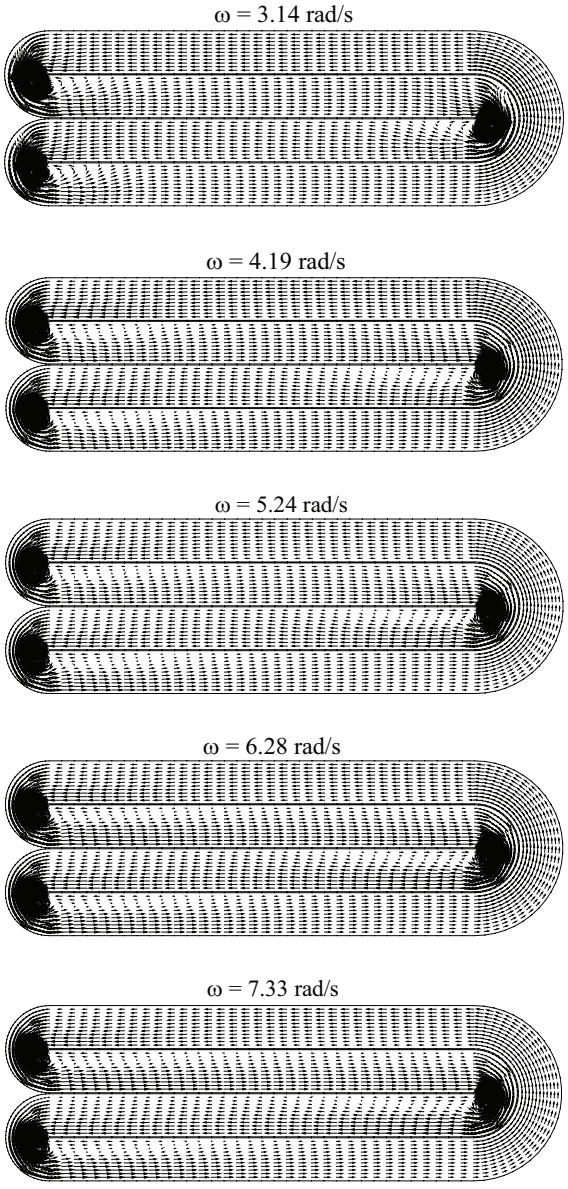

Fig. 4. Simulated velocity fields on the horizontal plane for different rotational speeds.

Table 1
Simulated average velocities of the flows with different rotational speeds of impellers

Average velocity over a cross-section V (m/s)	0.48	0.79	0.99	1.21	1.36
Rotational speed of impellers ω (1/s)	3.14	4.19	5.24	6.28	7.33
g/ω (m/s)	3.12	2.34	1.87	1.56	1.34

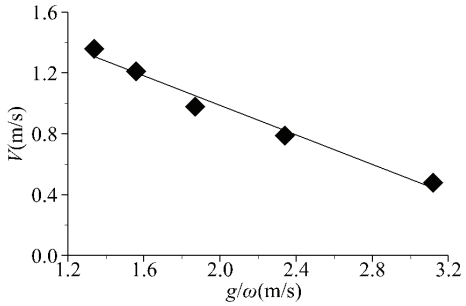

Fig. 5. Variation of V with g/ω.

4. Some discussions and further study plan

With a constant radius of impellers, a larger rotational speed of impellers will result in the average velocity of the flows to be increased. Therefore, according to the OD designing rule that the average fluid–velocity over a cross-section greater than 0.3 m/s is required, the rotational speed of impellers corresponding to the average velocity of 0.3 m/s should be determined, which will be useful for the efficiency of water treatment.

Dimensionless parameters significantly deepen our understanding of fluid-flow phenomena; even can provide some ways to find some laws of physical phenomena. By grouping significant quantities into dimensionless parameters it is possible to reduce the number of variables and to make this compact result (equations or data plots) applicable to all similar situations. Here, dimensional analysis method is used to find that the relationship between the average velocity of the flow and the rotational speed of impellers in an OD. Still, the coefficient of the relationship equation is obtained by the numerical simulation results. The relationship could be applicable for similar ODs. But for the similar ODs, the coefficients in the relationship maybe different, which should be determined by CFD or experiments.

Experiment is the main way to investigate a new basic phenomenon, taking a large amount of observation data as the foundation, still, the validation for a numerical simulation result must use the measured (in prototype or model) data [20]. Next, further study will be done to validate the simulation result by an experimental method. An experimental model for the actual Carrousel OD will be made of organic glass, according to the gravity similarity law (also named Froude number similarity theory) [12]. The experiment will be performed under the same working conditions used in the above simulations. The measured average velocities of the flows in the model are converted to that of the actual

Carrousel OD, and can be used to compare with the simulation results, and further, the reliability of the simulation results will be validated. Then, the CFD method can predict the flow fields in an OD with different rotational speeds of impellers, and can be used to determine a proper rotational speed of impellers.

5. Conclusions

In this paper, the dimensional analysis and numerical simulation methods are used to study the relationship between the average velocity of the flow and the rotational speed of impellers. According to the fitting of the points for the simulated results with different rotational speeds of impellers, the equation for the variation of V with g/ω can be approximately written as $V = -0.485\ g/\omega + 1.956$, with g/ω in the reference range of $1.34 < g/\omega < 3.0$, which is in agreement with the dimensional analysis result. The relationship could be applicable for similar ODs, in which the coefficients maybe different, which should be determined by CFD or experiments.

The effect of the rotational speeds of impellers on the flow fields was numerically simulated by the experimentally validated mathematical model in an OD. Next, further study will be done to validate the simulation results by an experimental method.

Acknowledgments

Financial support of this study was from the National Natural Science Foundation of China (Grant No. 51578452 and No. 51178391) and the scientific research projects of Shaanxi Province (2016GY-180, 2014K15-03-05).

Symbols

B	—	Width of the straight channel in the OD, m
C_μ	—	Model parameter in (5) with a value of 0.0845
C_1	—	Model parameter in (4)
C_2	—	Model parameter in (4) with a value of 1.68
g_i	—	Gravitational acceleration in i-th direction, $i = 1, 2, 3$, m/s^2
H	—	The water depth, m
k	—	Turbulent kinetic energy, m^2/s^2
p	—	Pressure, kg/m×s^2
P_k	—	Production term in (3) and (4)
r	—	Radius of impellers, m
R_1, R_2	—	Radius of bends, m
S	—	Parameter for computing C_1
$S_{i,j}$	—	Parameter for computing C_1
t	—	Time, s
u_i	—	Velocity component in i-th direction, $i = 1, 2, 3$, m/s
$U_i^{'}$	—	Fluctuating velocity component in i-th direction, $i = 1, 2, 3$, m/s
V	—	Averaged velocity over a cross-section, m/s
W	—	Velocity of the stationary reference frame, m/s
W_r	—	Velocity of the rotating reference frame, m/s
x_i	—	Space coordinate in i-th direction, $i = 1, 2, 3$, m

Greek

β	—	A constant of 0.015 for computing C_1
δ_{ij}	—	Kronecker function in (6), $\delta_{ij} = 1$ with $i = j$, and $\delta_{ij} = 0$ with $i \neq j$
ε	—	Kinetic energy dissipation rate, m^2/s^3
$\tilde{\eta}$	—	Parameter for computing C_1
$\tilde{\eta}_0$	—	A constant of 4.38 for computing C_1
μ	—	Molecular kinematic viscosity, kg/m×s
μ_t	—	Turbulent kinematic viscosity, kg/m×s
ρ	—	Density, kg/m^3
σ_k	—	Mod el parameter in (3) with a value of 0.7197
σ_ε	—	Model parameter in (4) with a value of 0.7197
π	—	Dimensionless number
ϕ	—	Dimensionless parameter
ω	—	Rotational speed, rad/s
ν	—	Viscosity of the water, kg/m×s

Subscripts

i, j	—	Direction, $i = 1, 2$, and 3; $j = 1, 2$, and 3
t	—	Turbulence

Abbreviations

CFD	—	Computational fluid dynamics
MRF	—	Multiple reference frame
N–S	—	Navier–Stokes
OD	—	Oxidation ditch
RNG	—	Renormalized group

References

[1] H. Wang, Y. Guo, Y. Hu, Simulation and improvement of flow fields in an oxidation ditch, Energy Environ., 2 (2009) 10–12.
[2] Zh. Chen, R. Yang, Numerical simulation of hydraulic characteristics of oxidation ditch with a new corrugated plate guide wall, Environ. Eng., 28 (2010) 33–44.
[3] L. Li, J. He, Q. Feng, Numerical simulation of guide plate influence on flow fields in an oxidation ditch, Environ. Sci. Technol., 37 (2014) 149–154.
[4] L. Fan, N. Xu, Zh. Wang, H. Shi, PDA experiments and CFD simulation of a lab-scale oxidation ditch with surface aerators, Chem. Eng. Res. Des., 88 (2010) 23–33.
[5] L. Li, J. Ni, Three-dimensional three-phase model for simulation of hydrodynamics, oxygen mass transfer, carbon oxidation, nitrification and denitrification in an oxidation ditch, Water Res., 53 (2014) 200–214.
[6] Y. Yang, J. Yang, J. Zuo, Y. Li, Sh. He, X. Yang, K. Zhang, Study on two operating conditions of a full-scale oxidation ditch for optimization of energy consumption and effluent quality by using CFD model, Water Res., 45 (2011) 3439–3452.
[7] Y. Liu, H.Ch. Shi, H.M. Shi, Zh. Wang, Study on a discrete-time dynamic control model to enhance nitrogen removal with fluctuation of influent in oxidation ditches, Water Res., 44 (2010) 5150–5157.
[8] Y.-q. Tang, J.-j. He, Q.-l. Liu, Numerical simulation of flow fields in an oxidation ditch with a submerged propeller as power, Chin. J. Hydrodyn., 3 (2013) 317–323.
[9] N. Yang, X. Wang, X. Guo, J. Liu, Structural optimization of guide-plates in an integrated oxidation ditch with a vertical circle, Acta Sci. Circum., 36 (2016) 914–919.
[10] L. Luo, W.M. Li, Y.S. Deng, T. Wang, Numerical simulation of a combined oxidation ditch flow using 3D k-epsilon turbulence model, J. Environ. Sci., 17 (2005) 808–812.
[11] H. Xie, J. Yang, Y. Hu, H. Zhang, Y. Yang, K. Zhang, X. Zhu, Y. Li, Ch. Yang, Simulation of flow field and sludge settling

in a full-scale oxidation ditch by using a two-phase flow CFD model, Chem. Eng. Sci., 109 (2014) 296–305.
[12] Zh.-g. Wu, Hydraulics, Higher Education Press, Beijing, 2003.
[13] W.-l. Wei, H.-c. Dai, Turbulence Model Theory and Engineering Applications, Shanxi Science and Technology Press, Xi'an, 2006.
[14] A.M. Karpinska, J. Bridgeman, CFD-aided modelling of activated sludge systems – a critical review, Water Res., 88 (2016) 861–879.
[15] A.M. Karpinska Portela, New Design Tools for Activated Sludge process, PhD Thesis, FEUP, University of Porto, Porto, Portugal, 2013.
[16] B.E. Launder, D.B. Spalding, The numerical computation of turbulent flows, Comput. Methods Appl. Mech. Eng., 3 (1974) 269–289.
[17] S.A. Orszag, I. Staroselsky, W.S. Flannery, Y. Zhang, Simulation and Modeling of Turbulent Flows, Chapter 4, Introduction to Renormalization Group Modeling of Turbulence, Oxford University Press Inc., New York, NY, USA, 1996.
[18] T.-H. Shih, W.W. Liou, A. Shabbir, Z. Yang, J. Zhu, A new k-ε eddy viscosity model for high Reynolds number turbulent flows, Comput. Fluids, 24 (1995) 227–238.
[19] W. Rodi, Turbulence Models and Their Application in Hydraulics, IAHR Monograph, CRC Press, Delft, The Netherlands, 1993.
[20] W. Wei, Y. Liu, B. Lv, Numerical simulation of optimal submergence depth of impellers in an oxidation ditch, Desal. Wat. Treat., 57 (2016) 8228–8235.